Large Area Films of Alternating Graphene−Carbon Nanotube Layers Processed in Water

Ferdinando Tristán-López,[†,||] Aaron Morelos-Gómez,[‡] Sofía Magdalena Vega-Díaz,[†] María Luisa García-Betancourt,[§] Néstor Perea-López,[§] Ana L. Elías,[§] Hiroyuki Muramatsu,[†] Rodolfo Cruz-Silva,[†] Shuji Tsuruoka,[†] Yoong Ahm Kim,[†,∞] Takuya Hayahsi,[‡] Katsumi Kaneko,[†] Morinobu Endo,[†,‡] and Mauricio Terrones[§,⊥,*]

[†]Research Center for Exotic Nanocarbons (JST), and [‡]Faculty of Engineering, Shinshu University, Wakasato 4-17-1, Nagano 380-8553, Japan and [§]Department of Physics and Center for 2-Dimensional and Layered Materials, and [⊥]Department of Chemistry, Department of Materials Science & Engineering, and Materials Research Institute, The Pennsylvania State University, 104 Davey Lababoratory, University Park, Pennsylvania 16802, United States. [||]Present address: Departamento de Ciencias Naturales (DCNI), División de Ciencias Naturales e Ingeniería, Universidad Autónoma Metropolitana (UAM), Unidad Cuajimalpa, 4871 Av. Vasco de Quiroga, Distrito Federal, 05300, México. [∞]Present address: Department of Polymer & Fiber System Engineering, Chonnam National University, 77 Yongbong-ro, buk-gu, Gwangju, 500-757, Korea.

ABSTRACT We report the preparation of hybrid paperlike films consisting of alternating layers of graphene (or graphene oxide) and different types of multiwalled carbon nanotubes (N-doped MWNTs, B-doped MWNTs, and pristine MWNTs). We used an efficient self-assembly method in which nanotubes were functionalized with cationic polyelectrolytes in order to make them dispersible in water, and subsequently these suspensions were mixed with graphene oxide (GO) suspensions, and the films were formed by casting/

evaporation processes. The electronic properties of these films (as produced and thermally reduced) were characterized, and we found electrical resistivities as low as 3×10^{-4} Ω cm. Furthermore, we observed that these films could be used as electron field emission sources with extraordinary efficiencies; threshold electric field of *ca.* 0.55 V/μm, β factor as high as of 15.19×10^3, and operating currents up to 220 μA. These values are significantly enhanced when compared to previous reports in the literature for other carbon nanostructured filmlike materials. We believe these hybrid foils could find other applications as scaffolds for tissue regeneration, thermal and conducting papers, and laminate composites with epoxy resins.
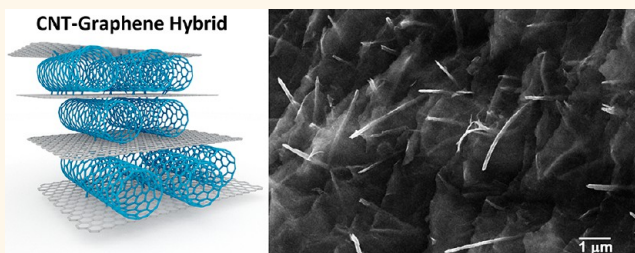
KEYWORDS: graphene · MWNT · graphene oxide · hybrid films · field emission · paper technology

A hybrid film could be defined as a film consisting of alternating layers of different types of nanostructures used as building blocks. These structures could be ordered or randomly distributed within each layer. For carbon materials, a hybrid film could be based on graphene or graphene oxide (GO) layers in conjunction with carbon nanotubes (CNTs). If CNTs intercalate between each individual graphene layer, the resulting hybrid films may possess enhanced physicochemical properties such as high surface area, mechanical robustness, and high electrical and thermal conduction, among others. Therefore, this controlled hybrid nanocarbon film fabrication has been a topic of recent research, and these films could be used in the fabrication of supercapacitors,[1] conducting electrodes,[2] solar cell components,[3] Li$^+$ batteries,[4] fuel cells,[5] and sensors.[6]

During the assembly of these carbon-based films, there are two main challenges to overcome: (1) the production of large area hybrid films without using supports or binders (*e.g.*, polymer or silicon) and (2) the synthesis of a homogeneous distribution of carbon nanotubes intercalated between individual graphene (or GO) sheets. So far, multiple approaches have been attempted with moderate success when fabricating such hybrid films: filtration,[7] casting from inorganic solutions,[8,9] electrophoretic deposition,[10,11] layer-by-layer (LbL) techniques,[12,13] and Langmuir−Blodgett techniques.[14] Unfortunately, many of these
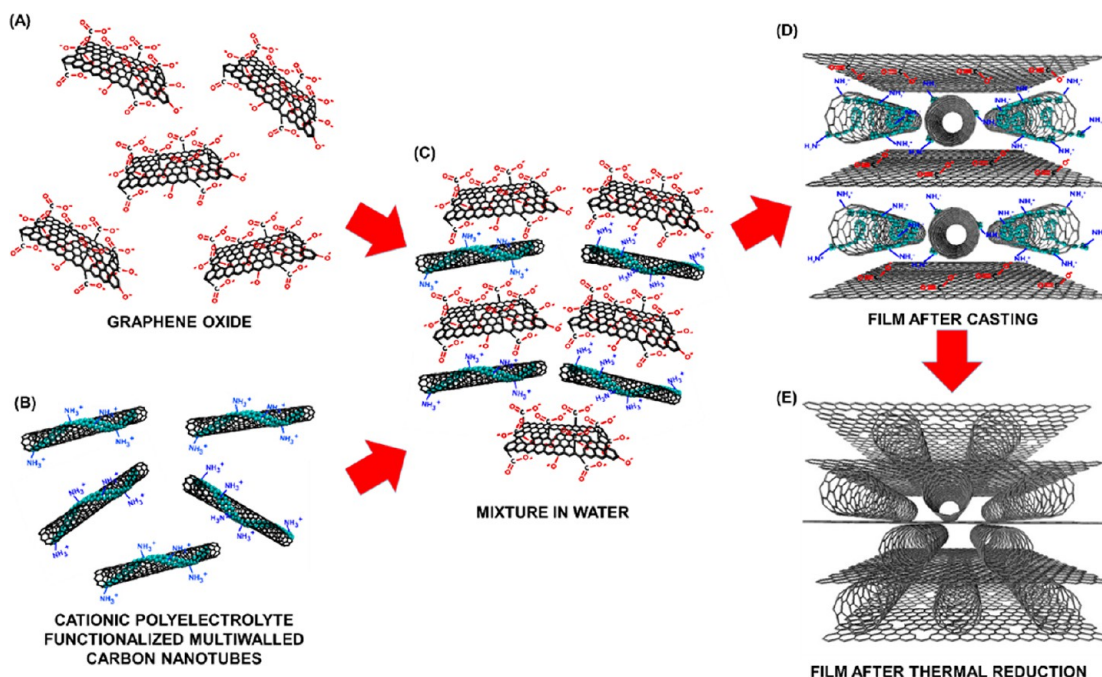
Figure 1. Schematics of the method developed in this work used to obtain hybrid films with different types of MWNTs (in particular N-doped MWNTs) and GO. The method consists in obtaining stable dispersions of CNTs and GO in water (steps A and B). Subsequently, these suspensions are mixed in a polar solvent to allow the interactions between CNTs and GO to occur (step C). This suspension with both components is cast on a mildly hot surface in order to remove the remaining solvent and allow the assembly of GO sheets with CNTs (step D). Finally the film could be reduced in order to obtain a stable reduced graphene−NT hybrid film (step E).

methods are time-consuming and face various obstacles during the processing because of the hydrophobic nature of carbon nanotubes and hydrophilic properties of GO (usually used as a precursor of graphene). To overcome these difficulties, chemical modification is used on either CNTs[12] or on graphene oxide (or reduced graphene oxide) sheets.[15] However, if the building blocks of these films quickly agglomerate, their electrical, thermal, transport properties will decrease significantly. Although surfactant free processing has been reported very recently,[16,17] all of these approaches are usually time-consuming and impractical when scaling up.

It is well-known that GO suspensions could act as a very good dispersing media of different carbon nanostructures. Despite this, there are only few examples reported in the literature that take advantage of these properties in order to obtain self-assembled hybrid carbon films.[1,9,18−20]

The use of polyelectrolytes has been successful to prepare layer-by-layer (LbL) hybrid films when mixing CNTs and GO sheets.[13] When the LbL technique is used, CNTs and GO nanosheets most of the time require severe chemical functionalization with ionic groups, thus making the electrostatic interaction the driving force controlling the morphology of the film during the self-assembly process.[2,12,13] However, the production of these films using this multistep method is again time-consuming and difficult to scale up.

In this work, we introduce and explore an efficient and facile self-assembly route to produce hybrid carbon films (graphene−NT paper) consisting of intercalated layers of individual multiwalled carbon nanotubes (MWNTs), nitrogen-doped MWNTs (N-MWNTs), or boron-doped MWNTs (B-MWNTs) with GO (or reduced GO—graphene), in aqueous dispersions assisted by cationic polyelectrolytes. This method takes advantage of two facts: (1) GO behaves as an anionic polyelectrolyte; thus by promoting subsequent ionic interactions with cationic polyelectrolyte functionalized CNTs in aqueous suspension, it is possible to bind CNTs to GO sheets; and (2) GO sheets tend to form stacked layered structures (*e.g.*, 3-D graphite) when the solvent is removed.[21] In particular, the use of cationic polyelectrolytes helps to break apart CNT bundles, thus increasing the amount of individual CNTs within suspensions. Since polyelectrolytes uniformly wrap CNTs, the anchorage of carbon nanotubes on GO sheets becomes efficient when compared to surfactants. Once the uniform aqueous suspensions are obtained, it is thus possible to assemble these GO/CNT/GO/CNT.../GO films after casting CNT/GO suspensions. It is noteworthy that the polyelectrolyte functionalized CNTs are electrostatically "anchored" to the GO sheets, and when the solvent is removed from the system (by evaporation), the GO sheets tend to adopt a layered
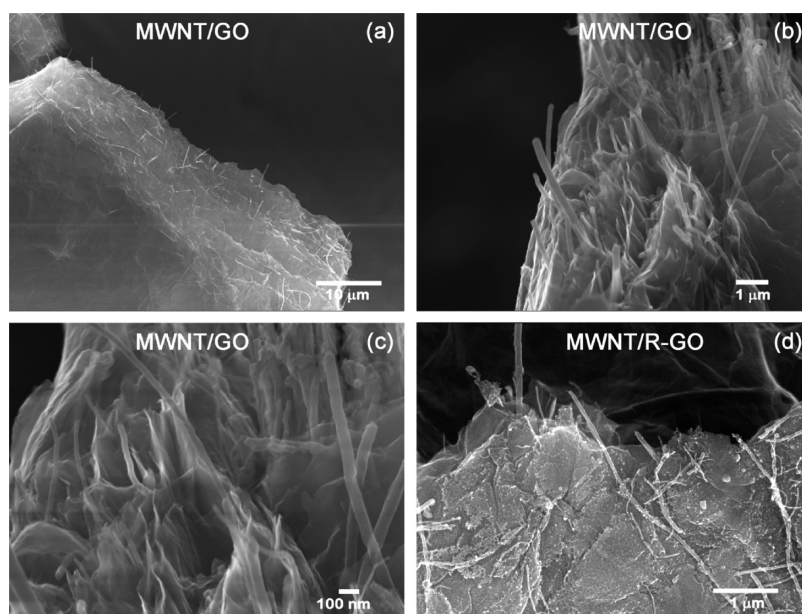
Figure 2. SEM images of MWNT/GO hybrid film: (a) pristine MWNT/GO film; (b and c) pristine film close up where only individual MWNTs are observed; (d) higher magnification of the film after thermal reduction at 800 °C in Ar flow (MWNT/R-GO).

morphology leaving CNTs trapped in between the layers, thus producing well stacked carbon hybrid films. Finally, these films could then be thermally reduced at high temperatures in order to obtain novel reduced graphene−CNT hybrid films exhibiting unprecedented properties (see Figure 1).

RESULTS AND DISCUSSION

After assembling the hybrid films from casting the mixed water suspensions of GO and MWNTs (MWNT, N-MWNT, or B-MWNT) they were characterized by different techniques. The micro-morphology of the films is depicted in Supporting Information, Figure S1. We noted that the films (hybrid paper) were mechanically stable and could be bent without experiencing failure (Figure S1a,b); they were twisted and bent and they could recoil to their original shape (Figure S1c,d).

By SEM, it was observed that the different types of MWNTs were randomly but uniformly distributed within different planes of the film; domains of aggregated MWNTs were notably absent (Figure 2A, Figure 3A, Figure 4A). From SEM images, it was also possible to observe that MWNTs were efficiently intercalated in between GO layers (Figure 2B, Figure 3B, and Figure 4B). The most important characteristic of these hybrid films is that no CNT bundles were observed, thus confirming that MWNTs were individually dispersed within the hybrid films. In addition, the cross-sectional edge of the hybrid paper revealed how carbon nanotubes were efficiently intercalated within GO sheets. (Figure 2C, Figure 3C, and Figure 4C) All these morphological features clearly indicate the successful synthesis of homogeneous hybrid paperlike films consisting of CNTs and GO.

After the thermal reduction of the films at 800 °C under an Ar flow, the morphology of the graphene− CNT film samples did not change significantly although the color turned from dark red brown to silvery black (see Figure 5). After this reduction, some MWNTs were exposed on the surface of the films but the layer-by-layer structure was preserved (Figure 2D, Figure 3D, and Figure 4D). We decided to carry out the thermal reduction of the films for two reasons: (1) to remove the binder molecules; in this case the cationic polyelectrolytes used to enhance the interactions of MWNTs in the GO sheets; and (2) to modify the electronic properties of GO by reduction to graphene, making it highly crystalline and electrically conducting.

Raman spectra presented in the Supporting Information (Figure S2) correspond to the pristine (as synthesized) hybrid films as well as the thermally reduced hybrid films. In all spectra, the D-band (1348 cm^{-1}, disorder vibrational mode due to the presence of non-sp^2-hybridized carbon atoms), G-band (1588 cm^{-1}, C−C stretching or tangential mode in graphitic lattices), 2D-band (2724 cm^{-1}), D+G (2918 cm^{-1}) and 2D' band (3151 cm^{-1}) were clearly identified. The presence of different types of MWNTs embedded within the hybrid films caused (in all the cases) a blue shift (∼2 cm^{-1}) in the D-band, whereas the G-band experienced a blue shift (∼3 cm^{-1}) only when pristine MWNTs were used; N- and B-MWNTs remained without change as shown in Table 1. The blue shift has been reported as part of the layer−layer interactions modifying the electronic environment of graphene.[22] We believe that this very small shift could be explained due to the charge transfer established between the
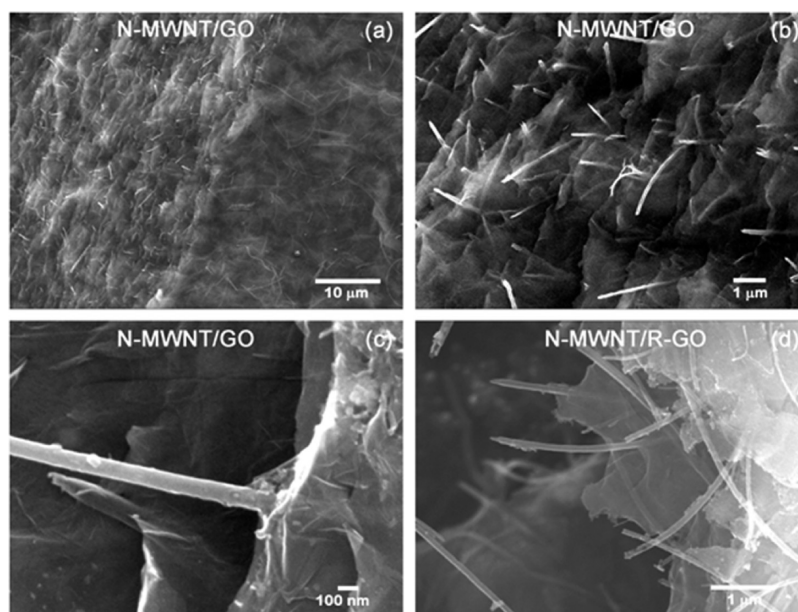
Figure 3. SEM images of N-MWNT/GO hybrid film: (a) pristine N-MWNT/GO film; (b and c) pristine film close up where only individual N-MWNT are observed; (d) close-up of the film after thermal reduction at 800 °C in Ar flow (N-MWNT/R-GO).
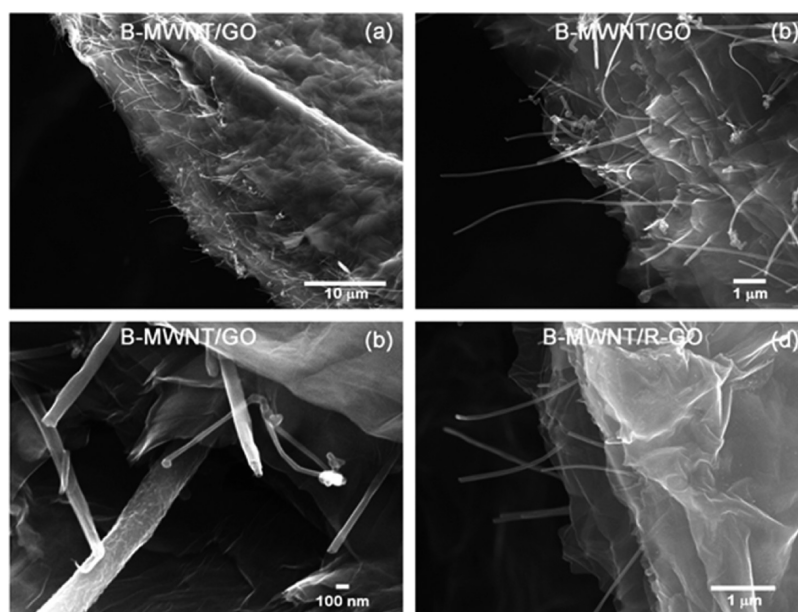

Figure 4. SEM images of B-MWNT doped/GO hybrid films (graphene-CNT powder): (a) pristine B-MWNT/GO film; (b and c) pristine film close up where only individual B-MWNT were observed; and (d) high magnification of the film after thermal reduction at 800 °C in Ar flow (B-MWNT/R-GO).

polyelectrolyte-coated MWNTs with the GO sheets. We also noted downshifts for N- and B-doped MWNTs films with GO. These downshifts confirm the n-type doping induced by nitrogen atoms, and also indicate an n-type doping in B-doped MWNTs GO systems caused by the large concentrations of polyelectrolyte, which contains N atoms.[23] For all reduced samples using doped MWNTs, the downshifts were slightly higher, thus confirming the presence of n-type hybrid systems. For pristine MWNT/GO hybrid films, there is a slight increase in the I_D/I_G ratio, which could be indicative of

the formation of sp^3-like hybridized carbon atoms established between GO (or reduced GO) and the MWNT walls. Note that the presence of non-sp^2-hybridized carbon atoms and dopants also breaks the perfect hexagonal symmetry of graphene and results in relatively large I_D/I_G ratios.[24] However, in our studies we observed that pristine MWNT/GO hybrid films exhibit the highest I_D/I_G ratios when compared to the other doped MWNTs and could be due to interconnections established between the GO, the polyelectrolyte, and the MWNT surface.
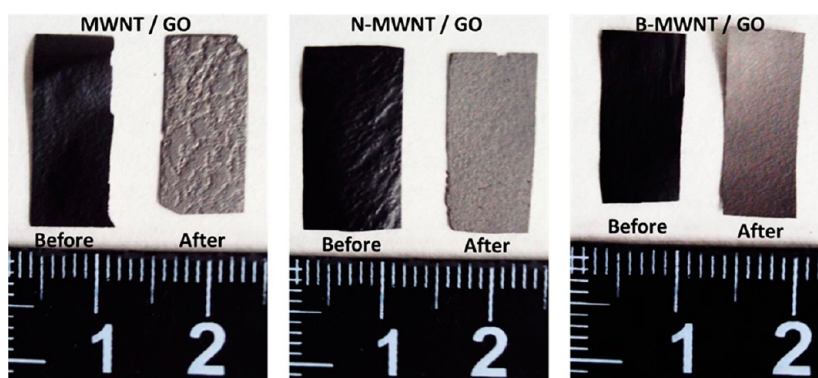
Figure 5. Hybrid paper macroscopic appearance after thermal reduction.

TABLE 1. Data Analysis Raman Spectroscopy

sample	Raman shift (cm^{-1})			Raman shift (cm^{-1})		
	D	G	I_D/I_G	2D	G+D	2D/G+D
GO	1348	1588	0.904	2724	2918	0.895
RGO	1349	1588	0.982	2697	2915	0.875
MWNT/GO	1350	1591	0.980	2717	2920	0.778
MWNT/R-GO	1350	1586	1.063	2710	2918	0.867
N-MWNT doped/GO	1350	1588	0.903	2693	2920	1.000
N-MWNT doped/R-GO	1349	1586	0.914	2689	2919	1.125
B-MWNT doped/GO	1350	1588	0.914	2693	2920	0.882
B-MWNT doped/R-GO	1350	1581	0.930	2682	2923	1.267

It is also noteworthy that all hybrid films made with MWNTs and GO exhibit an important red shift in the 2D-band. The decrease in intensity of the 2D-band is related to the formation of structural defects (including the presence of sp^3 hybridized carbon atoms) within the samples, which could be associated to the degree of oxidation of GO.[10,25] However, the intensity of these band changes significantly when MWNTs are introduced in the hybrid films. The value of the $I_{2D}/I_{(D+G)}$ ratio drastically decreases for MWNTs. Conversely, the $I_{2D}/I_{(D+G)}$ ratio increases in the hybrid film made with N- and B-MWNTs (see Table 1).

When all the films were thermally reduced at 800 °C, the Raman spectra of all the samples displayed changes associated with the reduction of GO films.[24] The I_D/I_G ratio increased in all cases. However for hybrid films containing B-MWNTs, the change in the I_D/I_G ratio is less evident (~0.010) when compared to the GO film or pristine MWNTs hybrid film (~0.080). This slight change can be due to the N or B dopants within nanotubes, thus meaning that doping is preserved after the thermal treatment of the paperlike films. However, more relevant changes were observed in the 2D-band, and these were related to the recovery of the sp^2 hybridized network in the reduced GO sheets. (2) While the $I_{2D}/I_{(D+G)}$ decreases for the MWNTs/R-GO film, this ratio increases significantly for B-MWNTs/R-GO and N-MWNTs/R-GO films (see Table 1). Therefore, MWNTs/R-GO films exhibit a higher degree of non-sp^2 "defects" and it could be related to the formation of interconnections established between GO (or graphene) with MWNTs within the hybrid films.

Figure 6A shows the thermogravimetric analysis (TGA) for all hybrid films as well as the control GO film; heating rate of 20 °C/min in a helium−oxygen 80/20 mixture from room temperature to 1000 °C. Besides the evident loss of water at the beginning of the thermogram, two steps were clearly identified in which a clear weight loss occurs (see Figure 6B). The first weight reduction appears at *ca.* 200 °C for all films, and it is associated to the exothermic process of GO reduction.[24,26] The second weight reduction corresponds to the oxidation process of graphite-like material present within the sample *ca.* 500 °C. Although it is very difficult to distinguish between the CNT and R-GO oxidation, this second loss is strongly influenced by the presence of CNTs during the process. It is clear that the pure GO film after reduction oxidizes very homogeneously at *ca.* 550 °C; the oxidation peak is sharp (Figure 6b). Interestingly, when doped MWNTs are embedded in the hybrid film matrix, the oxidation stability is significantly decreased. This is consistent with the presence of noncarbon defects in doped MWNTs.[27] Here the films were oxidized at temperatures below 550 °C (Figure 6b). It is important to point out that N-MWNTs/GO burns like a homogeneous material since it was only identified a single step in the thermogram. This could be attributed to a better interaction established between N-MWNTs and GO within the hybrid paper-like material. In this context, pristine MWNTs embedded in the hybrid film slightly increased the oxidation stability probably due to the establishment of covalent bonds (sp^3-like defects; see above) between the GO (or reduced GO) and MWNTs.

XPS analyses are shown in Figure 7 and Supporting Information, Figure S3. Here, it is possible to witness changes in the C and N bonding, with treated films before and after the thermal reduction at 800 °C. Figure 7 panels a−c show the C 1s core-level spectra and their deconvolutions used to determine the distribution of carbon electronic environments before reduction of each hybrid film studied in this work. The deconvoluted C 1s core-level spectra provide
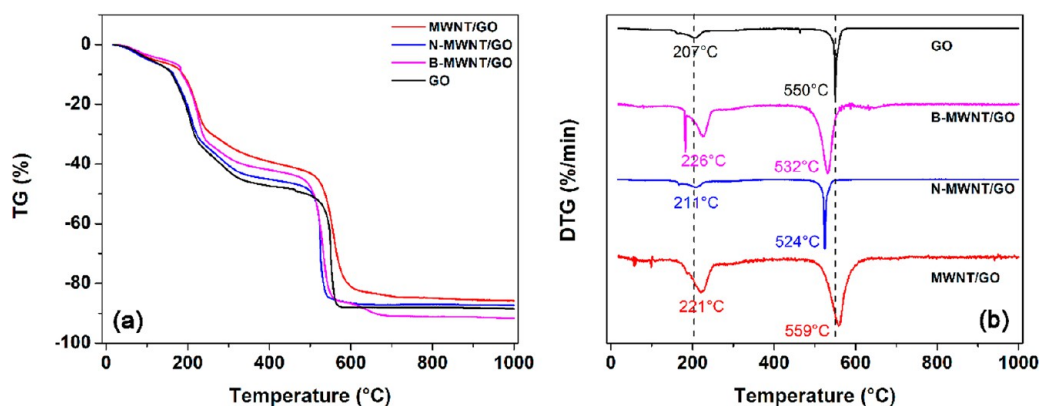
Figure 6. (a) Thermogravimetric analysis (TGA) of hybrid films in a helium−oxygen atmosphere (80:20) with a heating rate of 20 °C/min, and (b) first derivative (DTG) analysis of all hybrid films studied.
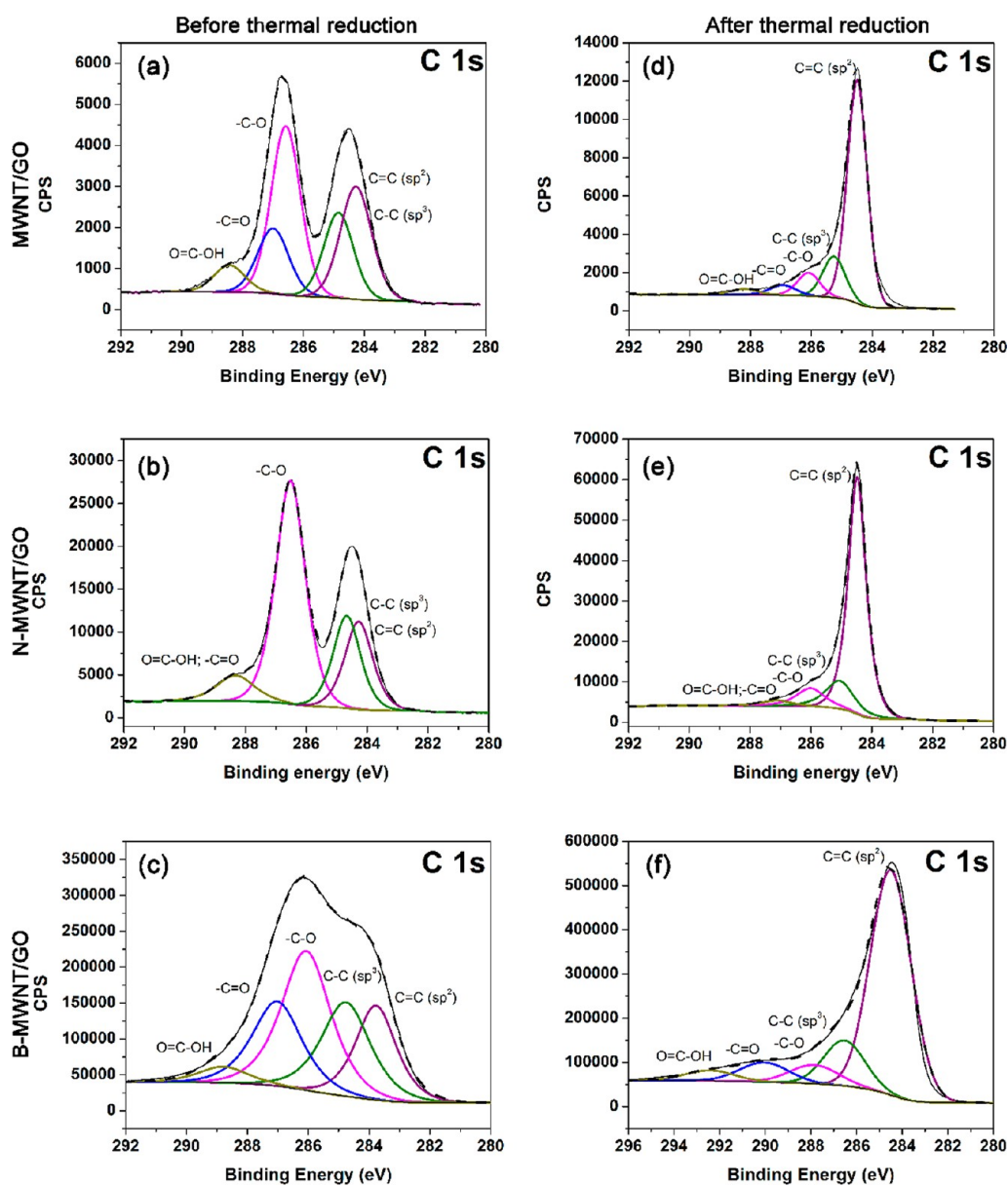

Figure 7. XPS spectra of different binding energies corresponding to the C 1s core-level: (a) pristine MWNT/GO film, (c) pristine N-MWNTs/GO film, and (e) pristine B-MWNTs/GO film; (b) MWNT/R-GO film, (d) N-MWNTs/R-GO, and (f) B-MWNTs/R-GO; all of them after thermal reduction at 800 °C in an Ar flow. Deconvoluted components are shown in color.

details about the surface functional groups present in MWNT/R-GO hybrid films, including sp^2-hybridized graphitic carbons (284.5 eV), sp^3-hybridized saturated carbons (∼285.0 eV), C—O (∼286.4 eV), C═O (∼287.8 eV), and carboxyl groups (288.9 eV), which are all in good agreement with previous works published in the literature.[2,28] It is clear from the C 1s core-level spectra that oxidized species are abundant before the thermal reduction, particularly carboxylic groups; and the sp^2 hybridization concentration is low in all film cases. The C 1s core-level spectra from pristine MWNT/GO and N-MWNT/GO films have similar spectral shapes, whereas the C 1s core-level spectrum only for the B-MWNTs/GO film seems to be different. However these differences could arise from the fact that the film has another distribution of oxygen groups; it has also to be considered, that the presence of the B—C bond perhaps is modifying this binding energy plot.

After reduction (Figure 7 panels d—f) the C 1s core-level spectra shows that oxidized species decrease their concentration and the sp^2 hybridization increases (a typical behavior after reducing GO). No significant differences were observed due to the presence of the different types of MWNTs in the GO/MWNTs hybrid materials. However these results confirm that the thermal reduction, under the conditions described above for hybrid materials, was indeed successful.

The N1s core-level spectra were also analyzed in order to monitor N doping. These are depicted in Supporting Information, Figure S3. Since different cationic polyelectrolytes were used to obtain stable dispersions of individual MWNTs, these cationic polyelectrolytes (all of them containing amino groups), were also present in the hybrid films and they enhanced electrostatic bonding interactions between MWNTs and the GO sheets after casting. During the thermal reduction treatment at 800 °C, it is expected that these polyelectrolytes were carbonized in the hybrid films. Since amino groups are present as part of the polyelectrolytes, it is expected that some of them could be incorporated as dopants within the graphitic network. After careful analysis of the N1s core-level spectra, it was clear that in all cases, nitrogen is present within the hybrid films after casting, mainly in the form of C—N bonding (see Supporting Information, Figures S3A—C). This is clearly due to the presence of cationic polyelectrolytes covering the nanotubes. The amount of nitrogen in each film after thermal reduction is different for each type of nanotube. The origin of different nitrogen content within the hybrid films could be explained in terms of the chemical affinity established between carbon nanotubes and the polyelectrolyte backbone experienced between dopants already contained within tubes (e.g., nitrogen or boron). Owing to this affinity, the amount of polyelectrolyte attached to the carbon nanotubes is expected to be different. For example nitrogen-doped

TABLE 2. Elemental Composition before and after Thermal Reduction Obtained by XPS

sample	before thermal reduction (%)			after thermal reduction (%)		
	carbon	oxygen	nitrogen	carbon	oxygen	nitrogen
MWNT/GO	71.8	27.5	0.7	88.8	11.2	
N-MWNT/GO	67.8	31.9	0.3	90.9	8.7	0.4
B-MWNT/GO[a]	71.7	28.1	0.1	94.6	3.4	0.9

[a] In this film the remaining percentage corresponds to the boron content due to the B-MWNT.

carbon nanotubes exhibit less amount of polyelectrolyte due to the nitrogen atoms present in the tube graphitic network, thus limiting the attachment of the nonpolar backbone of the polyelectrolyte. However, this effect is not expected for boron-doped or pristine carbon nanotubes, and these tubes are capable of immobilizing more polyelectrolyte chains with a subsequent increase in the amount of nitrogen that gets incorporated in the hybrid material after the thermal reduction of the films. Because of this reason, after the thermal treatment (see Supporting Information, Figures S3D—F), those films were also doped with nitrogen (MWNT/R-GO and B-MWNTs/R-GO), and nitrogen was mainly found in the form of C—N═C. This observation is due to decomposition of the polyelectrolytes during the thermal treatment, thus part of the nitrogen atoms got incorporated into the hybrid films as dopants.

Table 2 summarizes the elemental composition of the surface of the hybrid films before and after the treatment (reduction). It is worth mentioning two facts: First, the thermal reduction of the hybrid films was successful as indicated by the decrease of oxygen from around 30% to less than 12% in the reduced hybrid films, and even below 5% (B-MWNTs/R-GO). Second, nitrogen is present within films due to the presence of polyelectrolyte.

We carried out electrical conductivity measurements using the PPMS equipment, and also evaluated the electron field emission performance of the reduced films under vacuum.

From the resistivity measurements at room temperature we recorded resistivity values of 4.26×10^{-3} Ω cm for reduced pristine R-GO, whereas hybrid film containing MWNTs structures exhibited 0.30×10^{-3} Ω cm, 9.45×10^{-3} Ω cm, and 2.04×10^{-3} Ω cm for MWNTs/R-GO, N-MWNT/R-GO and B-MWNTs/R-GO, respectively; note that films consisiting of pristine MWNTs only exhibit resistivity values of 0.13 Ω cm. These low-resistivity values indicate that the incorporation of MWNTs could indeed enhance the electrical conductivity of R-GO; similar values have been reported for R-GO by Becerril and co-workers as well as Korkut and co-workers.[29,30] Supporting Information, Figure S4 shows all the resistivity data fitted using
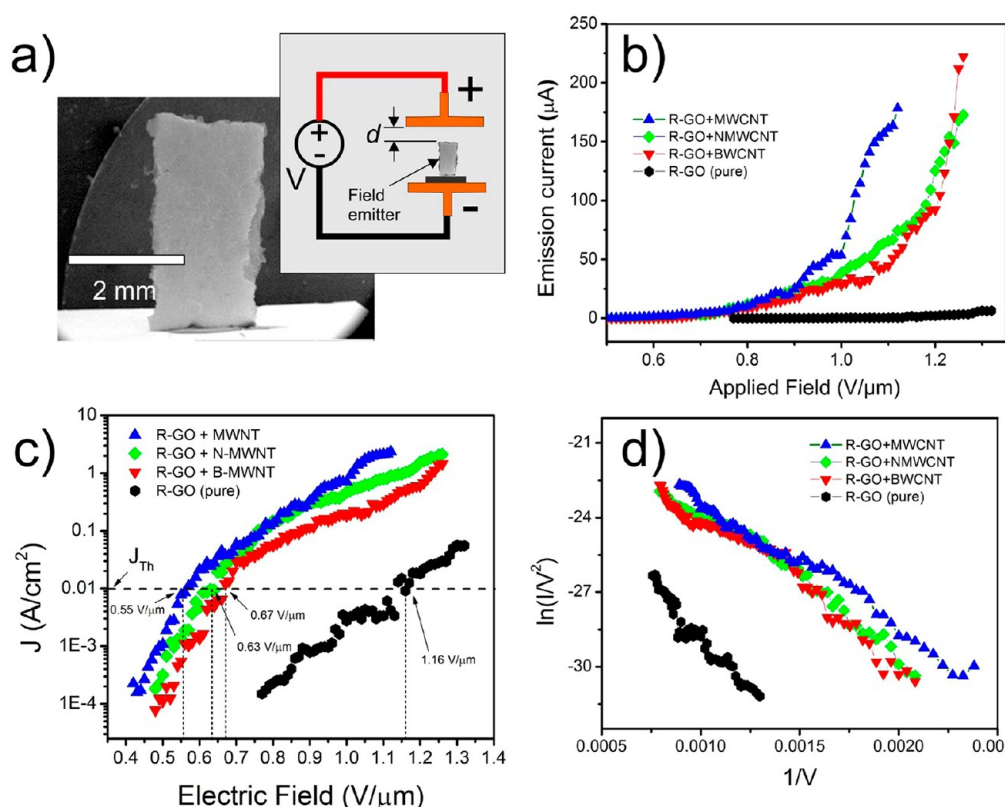
Figure 8. (a) SEM image of R-GO sheet shaped and mounted as a field emitter perpendicular to a conductive base and a simplified schematic of the FE setup, (b) $V-I$ plots of the different R-GO and R-GO+CNTs sheets used as electron emitters where maximum currents as high as 220 μA were registered. (c) $J-E$ plots where the threshold field (E_{Th}) can be extracted from the intersection of each plot with the current density value of 10 mA/cm^2 (J_{Th}). (d) Fowler–Norheim plots for all the R-GO film samples used to calculate each slope (s) to evaluate the corresponding field enhancement factor (β).

the variable range hopping model for Coulomb-gap variable range hopping, two-dimensional (2D-VRH) and three-dimensional (3D-VRH). The R-GO samples follow the variable range hopping model for two dimensions (2D-VRH) (see Supporting Information, Figure S4B), and when MWNTs are intercalated in the sheets, there is a strong-localization due to the dispersion of carbon nanotubes within the R-GO matrix resulting in Coulomb-gap VRH for temperatures ranging from 2 K to 300 K, 2 K to 50 K, and 2 K to 10 K for MWNT/R-GO, N-MWNTs/R-GO, and B-MWNT/R-GO, respectively (see Supporting Information, Figure S4A). Coulomb-gap VRH has been observed for disordered carbon nanostructures, such as fluorinated graphene and graphene nanoribbons.[31−35] In our case, the different MWNTs used could disrupt the continuity within the R-GO film, as well as the interface interactions established between MWNTs and R-GO. At temperatures of *ca.* 300 K, we obtained activation energies of 965, 394, 2560, and 2580 meV for R-GO, MWNTs/R-GO, N-MWNTs/R-GO, and B-MWNTs/R-GO, respectively. From these results we found that (1) initially, pristine R-GO films behave like a 2D-VRH semiconductor; (2) MWNT/R-GO films exhibit a lower resistivity and activation energy possibly due to the good interface interaction between MWNTs and R-GO (mediated

by the polyelectrolyte). This is also reflected in the homogeneous VRH behavior measured (2−300 K); (3) N-MWNTs/R-GO films exhibit a higher resistivity and activation energy than those observed for R-GO at room temperature. It has been shown by other groups that N doping may decrease the electrical resistivity; however, below certain nitrogen content the resistivity may also increase.[36,37] Another explanation for the low electrical transport is the strong variations in the charge distribution near the nitrogenated sites,[38,39] which affect negatively the resistivity of the N-MWNTs/R-GO hybrid films. However, at low temperatures (<20 K) the N-MWNTs/R-GO film exhibits the steepest slope for Coulomb-gap VRH (see Supporting Information, Figure S4A); here the nitrogen atoms may stop acting as electron-localization sites and could contribute to the electrical conductivity; (4) B-MWNT/R-GO films exhibit the highest activation energy, *ca.* 300 K, and steepest slope for Coulomb-gap VRH (see Supporting Information, Figure S4A), possibly because B has one electron less when compared to C and the charge density in the vicinity may favor electron localization.

The field emission of these reduced films was also measured (see Figure 8). We followed the procedure described by Perea-Lopez, N., *et al.*[40] The experiment consists of carefully mounting the hybrid film

TABLE 3. Dimensions of the Films and Threshold Field Values for the Reduced Hybrid Film Samples

sample	length (mm)	thickness (μm)	threshold field (V/μm)	β
R-GO	4.0	5.7	1.16	8.64×10^3
N-MWNTs/R-GO	3.7	4.1	0.63	14.38×10^3
B-MWNT/R-GO	4.5	7.7	0.67	13.80×10^3
MWNTs/R-GO	4.0	4.2	0.55	15.19×10^3

perpendicularly on a substrate (cathode) as shown in Figure 8a. This sample is introduced in a vacuum chamber at 10^{-8} Torr, and then the anode plate is moved to have a fixed vacuum gap of 1 mm between the emitter tip and the anode. The field emission properties including the threshold field (E_{TH}) and the field enhancement factor (β) were determined from the $J-E$ plots shown in Figure 8 panels c and d, and are also depicted in Table 3. From the Fowler−Norheim (F−N) model, the field enhancement factor, β, was obtained. This factor relates the local field at the emitter tip with the macroscopic field. Experimentally, β could be extracted by measuring the slope (s) of the linear region in the F−N plot by using the expression:

$$\beta = -B\varphi^{3/2}d/s$$

where the constant $B = B = 6.83 \times 10^9$ V eV$^{3/2}$ m^{-1}, φ is the work function, and d is the electrode separation distance.[40,41] To find the values in the expression described above, we assume the work function of graphitic carbon ($\varphi = 5$ eV), and $d = 1$ mm, which is the vacuum gap between the emitter and the anode during the field emission experiment.

By observing the field emission behavior of the vertically tested R-GO hybrid films, it is possible to notice that in the presence of nanotubes the threshold field values are significantly smaller (way below 1 V/μm) than that of the pure R-GO film ($\sim$1.16 V/μm). It means that they reach higher current densities with smaller applied electric field. The data showed that the hybrid reduced film with pristine MWNTs (MWNTs/R-GO) is the best emitter. The field enhancement factor was *ca.* 15.19×10^3 and the threshold field is *ca.*

0.55 V/μm. This result is consistent with the determination of resistivity values. The simplicity of making these films in addition to the easy way to make the emitters open up various possibilities to use our MWNTs/R-GO films as efficient field emitters in the fabrication of efficient light bulbs and flat panel and flexible displays. However, further research is needed along this direction in order to get a final emitter design based on R-GO+ MWCNTs hybrid films.

According to the morphology of the hybrid film edge (Figure 2a), where individual nanotubes are neatly exposed, it is expected that the global electron emission from the film's emitting edge is a contribution of the individual carbon nanotubes that act as individual and very efficient field emitters. Such a phenomenon is promoted by a multistage field enhancement effect as that observed by Huang and co-workers.[42]

CONCLUSIONS

Hybrid films consisting of MWNTs (pristine and doped) together with GO were successfully prepared in water solutions using cationic polyelectrolytes and GO suspensions. The use of nitrogen-containing cationic polyelectrolytes resulted in the doping of the films after thermal reduction. The method appears to be very advantageous in order to obtain a layered structure consisting of intercalated nanotubes within graphene sheets. After thermal reduction at 850 °C, the films retained the layered structure and their electronic properties were significantly enhanced due to the presence of MWNTs. These films not only possess a better electronic conduction but also seem to be excellent candidates for fabricating efficient field emission sources operating at low turn-on voltages, even better than standard CNTs. We strongly believe that our paper-like hybrid films could find important applications in the fabrication of Li-ion batteries[43] or supercapacitors owing to the possibility of having a three-dimensional conductive network for efficient charge transfer where the ions can have access since reduced graphene oxide cannot be restacked due to the presence of carbon nanotubes in between. Additional applications can be found in polymer composites and gas sensors, among others.

MATERIALS AND METHODS

Carbon Nanotube Synthesis. MWNTs and N-MWNTs were synthesized by the thermal decomposition of a solution containing 6 wt % ferrocene (Wako) in 94 wt % toluene or benzylamine, respectively. Both reagents were from Wako Chemicals and they are used as received in the synthesis of MWNTs by chemical vapor deposition (CVD) at atmospheric pressure as has been described elsewhere.[44,45] The MWNT synthesis was carried out at 825 °C in an Ar flow (2.5 L/min), while N-doped MWNT synthesis occurred at 850 °C in Ar flow as well (2.5 L/min).

B-doped MWNTs were synthesized as follows: The synthesis of carbon nanotubes was carried out in a vertical tubular reactor using ferrocene as a catalyst precursor, toluene as carbon

feedstock, and hydrogen as carrier gas in a semicontinuous system. A toluene solution containing a ferrocene compound (2−3 wt %) was fed into the reactor (diameter = 165 mm) with a rate of 25 g/min using a microfeeding pump. The reaction temperature was approximately 1200 °C. The as-synthesized tubes were mixed with boric acid (5 wt %) and then the mixture was thermally treated up to 2400 °C using a graphite furnace in an argon atmosphere

Graphene Oxide Synthesis. This material was synthesized from intercalated graphite (Wako), and a subsequent chemical oxidation described by Gilje *et al.*[46] This material was exhaustively washed with deionized water and then freezed dried in order to remove most of the trapped water.

Polyelectrolyte Functionalization. A simple route to functionalize MWNTs (pristine and doped) involved the use of cationic polyelectrolytes.[47−50] In particular, cationic polyelectrolytes allow a good dispersion of MWNTs in water. In addition, this method is able to efficiently debundle CNTs so that they become uniformly dispersed in the aqueous medium.

The procedure employed to carry out the polyelectrolyte functionalization involved 10 mg of MWNTs (SWNTs, DWNTs, N-doped MWNTs, and B-doped MWNTs) treated as follows. (1) The nanotube material was first thermally treated by an abrupt heating at 800 °C in an oxidative atmosphere (flowing air; 0.5 L/min) in order to remove amorphous carbon and remaining impurities from their surface (*e.g.*, solvents, hydrocarbons, *etc.*). It is expected that the surface of MWNTs would become slightly oxidized after this treatment, thus providing some additional anchoring sites that allow functionalization with cationic polyelectrolytes. (2) The resulting material was sonicated in water (HD 2070 ultrasound equipment) in order to obtain a homogeneous dispersion of MWNTs. This suspension was added drop by drop to a 2 mg/mL cationic polyelectrolyte solution (MWNT to polyethylenimine, M_w 60 000 − 70 000 Sigma-Aldrich; MWNT-N doped to polyallylamine, M_w 17 000; and MWNT-B doped with chitosan, medium M_w) under sonication in an ultrasonic bath. The latter process allowed the bundle fragmentation and results in homogeneous CNT dispersions functionalized with the cationic polyelectrolytes. (3) These CNTs were then washed by centrifugation−redispersion cycles in order to remove the excess cationic polyelectrolyte.

Hybrid Film Assembly. Once a stable suspension of 10 mg of polyelectrolyte functionalized CNTs (MWNTs, N-doped MWNTs, and B-doped MWNTs) is obtained, it is mixed drop by drop in 0.05 g/mL graphene oxide suspension under sonication. This mixture is kept under sonication for 30 additional minutes to allow a better intercalation of individual CNTs between individual GO sheets. Subsequently, this mixture was cast on a Teflon surface heated at 60 °C until a thin film is formed and could be easily detached from the surface. A blank sample consisting of a GO film was also prepared using the same procedure for comparative purposes. All films were thermally reduced at 800 °C under an Ar flow in order to produce the desired reduced graphene−CNT−reduced-graphene−CNT... hybrid films.

Hybrid Film Characterization Techniques. Pristine and thermally reduced hybrid films were characterized using different techniques: dynamic force microscopy (DFM), scanning electron microscopy (SEM, JEOL JSM-6335F), transmission electron microscopy (TEM), Raman spectroscopy (Renishaw Microraman, 532 nm line), thermogravimetric analysis (TGA, Rigaku Thermo-Mass Photo), X-ray photoelectron spectroscopy (XPS, Axis-Ultra, Kratos, Mg Kα line) and electrical resistivity (Cryogenic Probe Station, Lake Shore). After the films were thermally reduced, they were tested in order to determine their electrical transport (using a Physical Property Measurement System, PPMS) as well as their electron field emission properties, which was described by Perea-López *et al.*[40] All these techniques provide relevant and complementary information regarding these novel hybrid films including morphology, chemical composition and functional groups, air oxidation stability, electronic properties, *etc.*

Conflict of Interest: The authors declare no competing financial interest.

Supporting Information Available: Raman spectra for hybrid films; XPS spectra corresponding to the N 1s core-level; resistivity data analysis using different transport models. This material is available free of charge *via* the Internet at http://pubs.acs.org.

REFERENCES AND NOTES

1. Qiu, L.; Yang, X.; Gou, X.; Yang, W.; Ma, Z.-F.; Wallace, G. G.; Li, D. Dispersing Carbon Nanotubes with Graphene Oxide in Water and Synergistic Effects between Graphene Derivatives. *Chem.—Eur. J.* **2010**, *16*, 10653–10658.
2. Hong, T.-K.; Lee, D. W.; Choi, H. J.; Shin, H. S.; Kim, B.-S. Transparent, Flexible Conducting Hybrid Multilayer Thin Films of Multiwalled Carbon Nanotubes with Graphene Nanosheets. *ACS Nano* **2010**, *4*, 3861–3868.
3. Tung, V. C.; Chen, L.-M.; Allen, M. J.; Wassei, J. K.; Nelson, K.; Kaner, R. B.; Yang, Y. Low-Temperature Solution Processing of Graphene-Carbon Nanotube Hybrid Materials for High-Performance Transparent Conductors. *Nano Lett.* **2009**, *9*, 1949–1955.
4. Han, P.; Yue, Y.; Liu, Z.; Xu, W.; Zhang, L.; Xu, H.; Donga, S.; Cui, G. Graphene Oxide Nanosheets/Multiwalled Carbon Nanotubes Hybrid as an Excellent Electrocatalytic Material Towards VO_2^+/VO_2^+ Redox Couples for Vanadium Redox Flow Batteries. *Energy Environ. Sci.* **2011**, *4*, 4710–4717.
5. Lee, S. H.; Lee, D. H.; Lee, W. J.; Kim, S. O. Tailored Assembly of Carbon Nanotubes and Graphene. *Adv. Funct. Mater.* **2011**, *21*, 1338–1354.
6. Jeong, H. Y.; Lee, D.-S.; Choi, H. K.; Lee, D. H.; Kim, J.-E.; Lee, J. Y.; Lee, W. J.; Kim, S. O.; Choi, S.-Y. Flexible Room-Temperature NO_2 Gas Sensors Based on Carbon Nanotubes/Reduced Graphene Hybrid Films. *Appl. Phys. Lett.* **2010**, *96*, 213105.
7. Xu, Y.; Bai, H.; Lu, G.; Li, C.; Shi, G. Flexible Graphene Films *via* the Filtration of Water-Soluble Noncovalent Functionalized Graphene Sheets. *J. Am. Chem. Soc.* **2008**, *130*, 5856–5857.
8. Sun, X.; Sun, X.; Jin, J.; Wang, X.; Cai, D.; Song, M. J. Conductive Behavior and Self-Conductance Characteristic of Carbon Nanotubes/Functionalized Graphene Hybrid Films. *Nanosci. Nanotechnol.* **2011**, *11*, 5075–5082.
9. Cai, D.; Song, M.; Xu, C. Highly Conductive Carbon-Nanotube/Graphite-Oxide Hybrid Films. *Adv. Mater.* **2008**, *20*, 1706–1709.
10. Bon, S. B.; Valentini, L.; Kenny, J. M.; Peponi, L.; Verdejo, R.; Lopez-Manchado, M. A. Electrodeposition of Transparent and Conducting Graphene/Carbon Nanotube Thin Films. *Phys. Status Solidi A* **2011**, *207*, 2461–2466.
11. Wu, Z. S.; Pei, S.; Ren, W.; Tang, D.; Gao, L.; Liu, B.; Li, F.; Liu, C.; Cheng, H.-M. Field Emission of Single-Layer Graphene Films Prepared by Electrophoretic Deposition. *Adv. Mater.* **2009**, *21*, 1756–1760.
12. Byon, H. R.; Lee, S. W.; Chen, S.; Hammond, P. T.; Shao-Horn, Y. Thin Films of Carbon Nanotubes and Chemically Reduced Graphenes for Electrochemical Micro-Capacitors. *Carbon* **2011**, *49*, 457–467.
13. Yu, D.; Dai, L. Self-Assembled Graphene/Carbon Nanotube Hybrid Films for Supercapacitors. *J. Phys. Chem. Lett.* **2010**, *1*, 467–470.
14. Li, X. L.; Zhang, G.; Bai, X.; Sun, X.; Wang, X.; Wang, E.; Dai, H. Highly Conducting Graphene Sheets and Langmuir−Blodgett Films. *Nat. Nanotechnol.* **2008**, *3*, 538–542.
15. Park, J. S.; Cho, S. M.; Kim, W.-J.; Park, J.; Yoo, P. J. Fabrication of Graphene Thin Films Based on Layer-by-Layer Self-Assembly of Functionalized Graphene Nanosheets. *ACS Appl. Mater. Interfaces* **2011**, *3*, 360–368.
16. Azevedo, J.; Costa-Coquelard, C.; Jegou, P.; Yu, T.; Benattar, J.-J. Highly Ordered Monolayer, Multilayer, and Hybrid Films of Graphene Oxide Obtained by the Bubble Deposition Method. *J. Phys. Chem. C* **2011**, *115*, 14678–14681.
17. Tung, V. C.; Huang, J.-H.; Tevis, I.; Kim, F.; Kim, J.; Chu, C.-W.; Stupp, S. I.; Huang, J. Surfactant-Free Water-Processable Photoconductive All-Carbon Composite. *J. Am. Chem. Soc.* **2011**, *133*, 4940–4947.
18. Zhang, C.; Huang, S.; Tjiu, W. W.; Fana, W.; Liu, T. Facile Preparation of Water-Dispersible Graphene Sheets Stabilized by Acid-Treated Multiwalled Carbon Nanotubes and

Their Poly(Vinyl Alcohol) Composites. *J. Mater. Chem.* **2012**, *22*, 2427–2434.

19. Huang, Z. D.; Zhang, B.; Oh, S.-W.; Zheng, Q.-B.; Lin, X.-Y.; Yousefia, N.; Kim, J.-K. Self-Assembled Reduced Graphene Oxide/Carbon Nanotube Thin Films as Electrodes for Supercapacitors. *J. Mater. Chem.* **2012**, *22*, 3591–3599.

20. Kim, J.; Cote, L. J.; Kim, F.; Yuan, W.; Shull, K. R.; Huang, J. X. Graphene Oxide Sheets at Interfaces. *J. Am. Chem. Soc.* **2010**, *132*, 8180–8186.

21. Dikin, D. A.; Stankovich, S.; Zimney, E. J.; Piner, R. D.; Dommett, G. H. B.; Evmenenko, G.; Nguyen, S. T.; Ruoff, R. S. Preparation and Characterization of Graphene Oxide Paper. *Nature* **2007**, *448*, 457–460.

22. Wang, Y. Y.; Ni, Z. H.; Yu, T.; Shen, Z. X.; Wang, H. M.; Wu, Y. H.; Chen, W.; Wee, A. T. S. Raman Studies of Monolayer Graphene: The Substrate Effect. *J. Phys. Chem. C* **2008**, *112*, 10637–10640.

23. Campos-Delgado, J.; Maciel, I. O.; Cullen, D. A.; Smith, D. J.; Jorio, A.; Pimenta, M. A.; Terrones, H.; Terrones, M. Chemical Vapor Deposition Synthesis of N-, P-, and Si-Doped Single-Walled Carbon Nanotubes. *ACS Nano* **2010**, *4*, 1696–1702.

24. Stankovich, S.; Dikin, D. A.; Piner, R. D.; Kohlhaas, K. A.; Kleinhammes, A.; Jia, Y.; Wu, Y.; Nguyen, S. T.; Ruoff, R. S. Synthesis of Graphene-Based Nanosheets *via* Chemical Reduction of Exfoliated Graphite Oxide. *Carbon* **2007**, *45*, 1558–1565.

25. Jung, I.; Dikin, D. A.; Piner, R. D.; Ruosf, R. S. Tunable Electrical Conductivity of Individual Graphene Oxide Sheets Reduced at "Low" Temperatures. *Nano Lett.* **2008**, *8*, 4283–4287.

26. Lerf, A.; He, H.; Forster, M.; Klinowski, J. Structure of Graphite Oxide Revisited. J. *Phys. Chem. B* **1998**, *102*, 4477–4482.

27. Bom, D.; Andrews, R.; Jacques, D.; Anthony, J.; Chen, B.; Meier, M. S.; Selegue, J. P. Thermogravimetric Analysis of the Oxidation of Multiwalled Carbon Nanotubes: Evidence for the Role of Defect Sites in Carbon Nanotube Chemistry. *Nano Lett.* **2002**, *2*, 615–619.

28. Mattevi, C.; Eda, G.; Agnoli, S.; Miller, S.; Mkhoyan, K. A.; Celik, O.; Mastrogiovanni, D.; Granozzi, G.; Garfunkel, E.; Chhowalla, M. Evolution of Electrical, Chemical, and Structural Properties of Transparent and Conducting Chemically Derived Graphene Thin Films. *Adv. Funct. Mater.* **2009**, *19*, 2577–2583.

29. Becerril, H. A.; Mao, J.; Liu, Z.; Stoltenberg, R. M.; Bao, Z.; Chen, Y. Evaluation of Solution-Processed Reduced Graphene Oxide Films as Transparent Conductors. *ACS Nano* **2008**, *2*, 463–470.

30. Korkut, S.; Roy-Mayhew, J. D.; Dabbs, D. M.; Milius, D. L.; Aksay, I. A. High Surface Area Tapes Produced with Functionalized Graphene. *ACS Nano* **2011**, *5*, 5214–5222.

31. Withers, F.; Bointon, T. H.; Dubois, M.; Russo, S.; Craciun, M. F. Nanopatterning of Fluorinated Graphene by Electron Beam Irradiation. *Nano Lett.* **2011**, *11*, 3912–3916.

32. Jang, W. Y.; Kulkarni, N. N.; Shih, C. K.; Yao, Z. Electrical Characterization of Individual Carbon Nanotubes Grown in Nanoporous Anodic Alumina Templates. *Appl. Phys. Lett.* **2004**, *84*, 1177–1179.

33. Wang, D. P.; Feldman, D. E.; Perkins, B. R.; Yin, A. J.; Wang, G. H.; Xu, J. M.; Zaslavsky, A. Hopping Conduction in Disordered Carbon Nanotubes. *Solid State Commun.* **2007**, *142*, 287–291.

34. Danneau, R.; Wu, F.; Tomi, M. Y.; Oostinga, J. B.; Morpurgo, A. F.; Hakonen, P. J. Shot Noise Suppression and Hopping Conduction in Graphene Nanoribbons. *Phys. Rev. B* **2010**, *82*, 161405.

35. Han, M. Y.; Brant, J. C.; Kim, P. Electron Transport in Disordered Graphene Nanoribbons. *Phys. Rev. Lett.* **2010**, *104*, 056801.

36. Derradji, N. E.; Mahdjoubi, M. L.; Belkhir, H.; Mumumbila, N.; Angleraud, B.; Tessier, P. Y. Nitrogen Effect on the Electrical Properties of CNx Thin Films Deposited by Reactive Magnetron Sputtering. *Thin Solid Films* **2005**, *482*, 258–263.

37. Monclus, M. A.; Cameron, D. C.; Chowdhurry, A. K. M. S. Electrical Properties of Reactively Sputtered CNx Films. *Thin Solid Films* **1999**, *341*, 94–100.

38. Cruz-Silva, E.; Cullen, D. A.; Gu, L.; Romo-Herrera, J. M.; Muñoz-Sandoval, E.; López-Urías, F.; Sumpter, B. G.; Meunier, V.; Charlier, J.-C.; Smith, D. J.; *et al.* Heterodoped Nanotubes: Theory, Synthesis, and Characterization of Phosphorus–Nitrogen Doped Multiwalled Carbon Nanotubes. *ACS Nano* **2008**, *2*, 441–448.

39. Gracia-Espino, E.; López-Urías, F.; Terrones, H.; Terrones, M. Doping (10, 0)-Semiconductor Nanotubes with Nitrogen and Vacancy Defects. *Mater. Express* **2011**, *1*, 127–135.

40. Perea-López, N.; Rebollo-Plata, B.; Briones-León, J. A.; Morelos-Gómez, A.; Hernández-Cruz, D.; Hirata, G. A.; Meunier, V.; Botello-Méndez, A. R.; Charlier, J. C.; Maruyama, B.; et al. Millimeter-Long Carbon Nanotubes: Outstanding Electron-Emitting Sources. *ACS Nano* **2011**, *5*, 5072–5077.

41. Gao, H.; Mu, C.; Wang, F.; Xu, D.; Wu, K.; Xie, Y.; Liu, S.; Wang, E.; Xu, J.; Yu, D. Field Emission of Large-Area and Graphitized Carbon Nanotube Array on Anodic Aluminum Oxide Template. *J. Appl. Phys.* **2003**, *93*, 5602–5605.

42. Huang, J. Y.; Kempa, K.; Jo, S. H.; Chen, S.; Ren, Z. F. Giant Field Enhancement at Carbon Nanotube Tips Induced by Multistage Effect. *Appl. Phys. Lett.* **2005**, *87*, 053110.

43. Lee, S.-H.; Sridhar, V.; Jung, J.-H.; Karthikeyan, K.; Lee, Y.-S.; Mukherjee, R.; Koratkar, N.; Oh, I.-K. Graphene-Nanotube-Iron Hierarchichal Nanostructure as Lithium Ion Battery. *ACS Nano* **2013**, *7*, 4242–4251.

44. Terrones, M.; Ajayan, P. M.; Banhart, F.; Blase, X.; Carroll, D. L.; Charlier, J. C.; Czerw, R.; Foley, B.; Grobert, N.; Kamalakaran, R.; *et al.* N-Doping and Coalescence of Carbon Nanotubes: Synthesis and Electronic Properties. *Appl. Phys. A: Mater. Sci. Process.* **2002**, *74*, 355–361.

45. Mayne, M.; Grobert, N.; Terrones, M.; Kamalakaran, R.; Rühle, M.; Kroto, H. W.; Walton, D. R. M. Pyrolytic Production of Aligned Carbon Nanotubes from Homogeneously Dispersed Benzene-Based Aerosols. *Chem. Phys. Lett.* **2001**, *338*, 101–107.

46. Gilje, S.; Han, S.; Wang, M.; Wang, K. L.; Kaner, R. B. A Chemical Route to Graphene for Device Applications. *Nano Lett.* **2007**, *7*, 3394–3398.

47. Rubianes, M. D.; Rivas, G. A. Dispersion of Multiwall Carbon Nanotubes in Polyethylenimine: A New Alternative for Preparing Electrochemical Sensors. *Electrochem. Commun.* **2007**, *9*, 480–484.

48. Poloniemi, H.; Aäritalo, T.; Laiho, T.; Liuke, H.; Kocharova, N.; Haapakka, K.; Terzi, F.; Seeber, R.; Lukkari, J. Water-Soluble Full-Length Single-Wall Carbon Nanotube Polyelectrolytes: Preparation and Characterization. *J. Phys. Chem. B* **2005**, *109*, 8634–8642.

49. Kim, B.; Park, H.; Sigmund, W. M. Electrostatic Interactions between Shortened Multiwall Carbon Nanotubes and Polyelectrolytes. *Langmuir* **2003**, *19*, 2525–2527.

50. Duesberg, G. S.; Burghard, M.; Muster, J.; Philipp, G. Separation of Carbon Nanotubes by Size Exclusion Chromatography. *Chem. Commun.* **1998**, *67*, 435–436.